

# A Solution-Processable High-Modulus Crystalline Artificial Solid Electrolyte Interphase for Practical Lithium Metal Batteries

Zhiao Yu, Samuel Seo,\* Jongchan Song, Zewen Zhang, Solomon T. Oyakhire, Yang Wang, Rong Xu, Huaxin Gong, Song Zhang, Yu Zheng, Yuchi Tsao, Luca Mondonico, Eder G. Lomeli, Xinchang Wang, Wonkeun Kim, Kyoungan Ryu, and Zhenan Bao\*

The solid electrolyte interphase (SEI) has been identified as a key challenge for Li metal anodes. The brittle and inhomogeneous native SEI generated by parasitic reactions between Li and liquid electrolytes can devastate battery performance; therefore, artificial SEIs (ASEIs) have been proposed as an effective strategy to replace native SEIs. Herein, as a collaboration between academia and industrial R&D teams, a multifunctional (crystalline, high modulus, and robust, Li<sup>+</sup> ion conductive, electrolyte-blocking, and solution processable) ASEI material, LiAl-FBD (where “FBD” refers to 2,2,3,3-tetrafluoro-1,4-butanediol), for improving Li metal battery performance is designed and synthesized. The LiAl-FBD crystal structure consists of Al<sup>3+</sup> ions bridged by FBD<sup>2-</sup> ligands to form anion clusters while Li<sup>+</sup> ions are loosely bound at the periphery, enabling an Li<sup>+</sup> ion conductivity of  $9.4 \times 10^{-6} \text{ S cm}^{-1}$ . The fluorinated, short ligands endow LiAl-FBD with electrolyte phobicity and high modulus. The ASEI is found to prevent side reactions and extend the cycle life of Li metal electrodes. Specifically, pairing LiAl-FBD coated 50  $\mu\text{m}$  thick Li with industrial 3.5  $\text{mAh cm}^{-2}$  NMC811 cathode and 2.8  $\mu\text{L mAh}^{-1}$  lean electrolyte, the Li metal full cells show superior cycle life compared to bare ones, achieving 250 cycles at 1  $\text{mA cm}^{-2}$ .

Particularly, the issue originates from the high reactivity of Li metal and thus continuous parasitic reactions between Li and electrolyte components that finally result in a poorly passivating layer, known as solid-electrolyte interphase (SEI).<sup>[3–6]</sup> Generally, the native SEIs in conventional/commercial carbonate electrolytes are mechanically brittle, heterogeneous in ionic conduction, and fail to passivate the Li surface during long-term cycling.

To solve these issues associated with Li metal anodes, several strategies have been proposed, such as liquid electrolyte engineering,<sup>[7–14]</sup> solid-state electrolytes,<sup>[15–18]</sup> Li metal hosts,<sup>[5,19]</sup> or pretreatment of Li metal.<sup>[20–22]</sup> Artificial SEIs (ASEIs)<sup>[23–28]</sup> have garnered increasing attention due to their potential compatibility with commercial electrolytes<sup>[24]</sup> and the possibility for scalable manufacturing.<sup>[23]</sup> Particularly, it is critical to develop production-friendly solution-processable ASEIs for Li metal anodes, so that the ASEIs can be implemented through scalable coating methods,<sup>[29]</sup> such as spray coating, slot-die coating, gravure coating, or inkjet printing.

In addition to the aforementioned practical considerations, the physical and chemical properties of ASEIs can be rationally designed to overcome the drawbacks of native SEIs. Several key features of ASEIs have been identified as essential to protect Li metal anode,<sup>[4,28,30–34]</sup> such as high ionic conductivity,

## 1. Introduction

Lithium (Li) metal anode is regarded as one of the most promising negative electrodes for next-generation batteries due to its potential in delivering high energy density.<sup>[1,2]</sup> However, the poor cyclability of Li metal anode is a long-standing issue that prohibits its implementation in realistic energy storage devices.

Z. Yu, S. T. Oyakhire, H. Gong, S. Zhang, Y. Zheng, Y. Tsao, L. Mondonico, Z. Bao  
Department of Chemical Engineering  
Stanford University  
Stanford, CA 94305, USA  
E-mail: zbao@stanford.edu  
Z. Yu, Y. Zheng, Y. Tsao  
Department of Chemistry  
Stanford University  
Stanford, CA 94305, USA

S. Seo, J. Song, W. Kim, K. Ryu  
Advanced Battery Development Team 1  
Hyundai Motor Company  
Uiwang, Gyeonggi 16092, Republic of Korea  
E-mail: seosam@hyundai.com

Z. Zhang, Y. Wang, R. Xu, Y. Tsao, E. G. Lomeli  
Department of Materials Science and Engineering  
Stanford University  
Stanford, CA 94305, USA

X. Wang  
School of Electronic Science and Engineering  
State Key Laboratory of Physical Chemistry of Solid Surface  
Xiamen University  
Xiamen, Fujian 361005, P. R. China

 The ORCID identification number(s) for the author(s) of this article can be found under <https://doi.org/10.1002/aenm.202201025>.

DOI: 10.1002/aenm.202201025

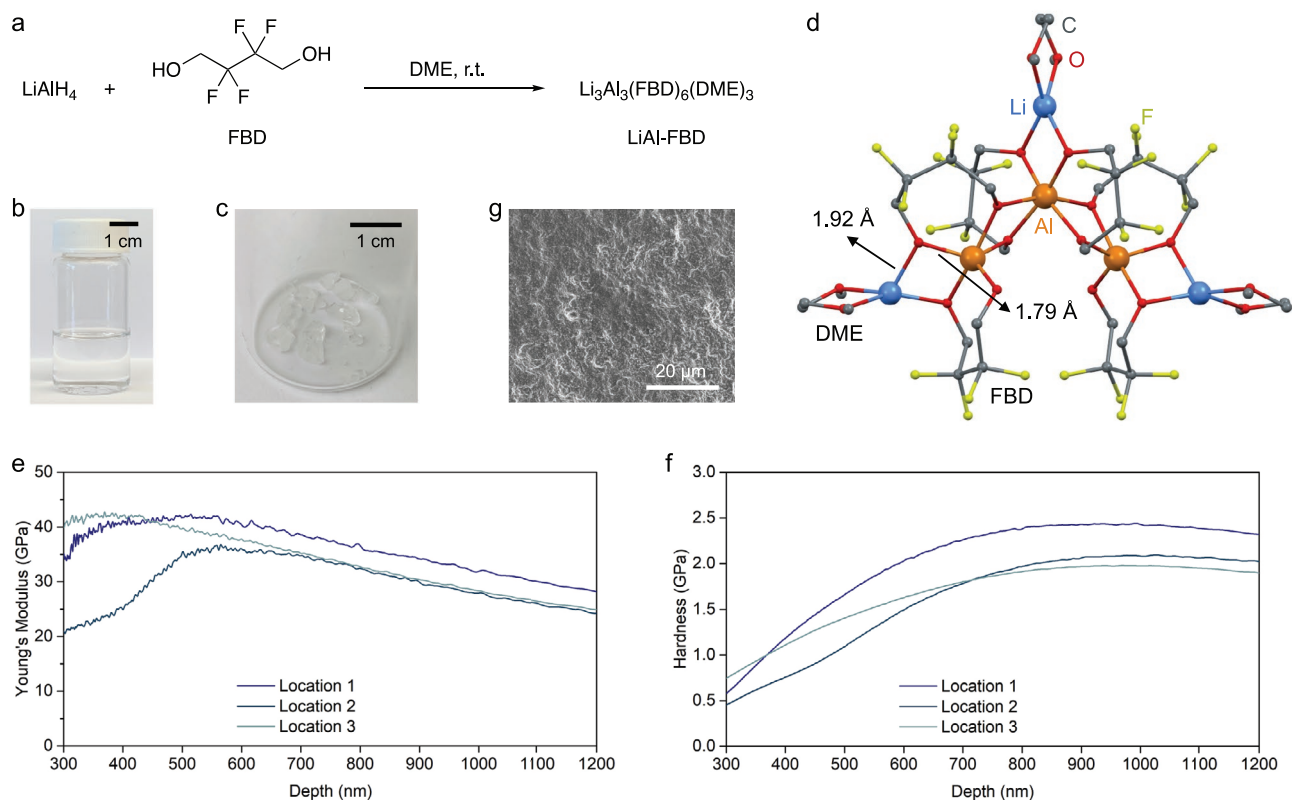


**Figure 1.** a) Synthesis of LiAl-FBD. b) Optical image of LiAl-FBD solution. c, d) Optical image and refined crystal structure of LiAl-FBD. Nanoindentation measurements showing the e) Young's modulus and f) hardness of LiAl-FBD material. g) SEM image of coated LiAl-FBD on Li foil.

good mechanical stability and electrolyte-phobic feature. As elaborated in the previous reports,<sup>[24,30,32]</sup> the incorporation of all the desired properties into one multifunctional ASEI material system can be challenging; therefore, synergistic effects are needed to further achieve realistic Li metal batteries.

## 2. Main Text

Herein, we design and synthesize a solution-processable, mechanically strong, Li-ion conductive, and electrolyte-blocking ASEI material based on the product of an instantaneous reaction between  $\text{LiAlH}_4$  and 2,2,3,3-tetrafluoro-1,4-butanediol (FBD) in 1,2-dimethoxyethane (DME) (Figure 1a and Methods, Supporting Information). After  $\text{H}_2$  gas releasing as the only by-product, deprotonation of FBD was confirmed by nuclear magnetic resonance (NMR) spectroscopy (Figures S1–S3, Supporting Information). The obtained species,  $\text{LiAl}(\text{FBD})_2$  in a simplified formula, was found to be soluble in DME to form a colorless solution (Figure 1b), which can be directly coated into thin films. Large crystals, millimeter- to centimeter-scale, can be readily obtained after solvent evaporation as shown in Figure 1c. The crystal structure was solved from single-crystal X-ray diffraction (SCXRD) data and was further refined to be  $\text{Li}_3\text{Al}_3(\text{FBD})_6(\text{DME})_3$  (Figure 1d and Figure S4 and Table S1, Supporting Information). Due to the moderate length of  $\text{FBD}^{2-}$  ligand, this crystal structure is composed of a large anion

cluster which is composed of three  $\text{Al}^{3+}$  cations as the centers and six deprotonated  $\text{FBD}^{2-}$  as the bridges/ligands to link those  $\text{Al}^{3+}$  centers. Similar yet smaller-sized  $\text{Al}^{3+}$ -diol coordination was previously observed.<sup>[35]</sup> The  $^1\text{H}$ - and  $^{19}\text{F}$ -NMR spectra also indicate a multistate clustering feature as evidenced by the broadened peaks (Figures S1 and S2, Supporting Information). Interestingly, the three  $\text{Li}^+$  ions are located at the periphery of the cluster, chelated by one DME solvent molecule for each. The O atoms on deprotonated  $\text{FBD}^{2-}$  exhibit a longer distance with  $\text{Li}^+$  (1.92 Å) than with  $\text{Al}^{3+}$  (1.79 Å), indicating their loose coordination with  $\text{Li}^+$  yet stronger binding with  $\text{Al}^{3+}$ . Such a feature should free  $\text{Li}^+$  ions, confirmed by its high ionic conductivity for a crystalline material (up to  $9.4 \times 10^{-6} \text{ S cm}^{-1}$  at room temperature, Figure S5, Supporting Information), and enables ion transport through the ASEI when implemented on Li metal surface. Furthermore, compared to our previous report<sup>[24]</sup> using long ligands, the short fluorinated FBD ligands not only provide higher  $\text{Li}^+$  concentration (2 wt% for LiAl-FBD vs 0.8 wt% in the previous report<sup>[24,30]</sup>) in the ASEI to prevent  $\text{Li}^+$  depletion but also enhance mechanical strength and electrolyte-blocking feature as will be elaborated later.

The mechanical strength and robustness of LiAl-FBD material were measured by nanoindentation tests.<sup>[36]</sup> As shown in Figure 1e,f, LiAl-FBD exhibited high Young's modulus (30–40 GPa in stable region) and hardness (>2 GPa in stable region). These moduli are much higher than those of previously reported polymer ASEIs.<sup>[27,37]</sup> A modulus over 4 GPa

was usually hypothesized to be effective to suppress Li dendrites,<sup>[32,36]</sup> and thus such mechanical strength of LiAl-FBD is a desirable feature for its Li metal protection effect as will be discussed in the later section.

In addition to characterizing the crystalline LiAl-FBD material, its feasibility as a crystalline coating layer was confirmed by scanning electron microscope (SEM). As shown in Figure 1g and Figure S6 (Supporting Information), a conformal protection layer with a thickness of  $\approx 500$  nm was observed on a thin Li foil. The crystalline nature of LiAl-FBD coating was supported by polarized optical microscope and grazing-incidence wide-angle X-ray scattering (GIWAXS) (Figure S7, Supporting Information). The LiAl-FBD ASEI on Li foil was dip-coated from the solution (Methods, Supporting Information) and is potentially compatible with solution-based large-scale processing methods as mentioned above.

After confirming its feasibility as a conformal ASEI, LiAl-FBD coating was investigated in batteries to confirm its effectiveness in Li metal protection. Conventional carbonate-based electrolyte 1 M LiPF<sub>6</sub> in ethylene carbonate (EC)/dimethyl carbonate (DMC) (denoted as LP30) + 2% vinylene carbonate (VC) + 10% fluoroethylene carbonate (FEC) was used here to examine the effectiveness of LiAl-FBD coating in the commercial, scalable, low-cost electrolyte that is not Li metal compatible though.

The Li | Li symmetric cells were first used to examine the electrolyte-blocking feature with LiAl-FBD coating. As shown by the Nyquist plots of electrochemical impedance spectroscopy (EIS, Figure 2a,b and Figure S8, Supporting Information), the bare Li | Li symmetric cell showed continuous and drastic increase in impedance immediately after the cell assembling ( $\approx 800 \Omega$ ) to 32 h ( $\approx 1500 \Omega$ ); by contrast, the LiAl-FBD protected Li | Li symmetric cell maintained low and stable interfacial impedance over the whole cell resting time, i.e., only increasing from  $\approx 100$  to  $\approx 180 \Omega$ . In addition to EIS evolution over time, the cycling behavior of LiAl-FBD coated Li | Li symmetric cell is far more stable than bare Li one (Figure 2c). The coated cell was cycled for more than 1000 h (500 cycles) without significant polarization or short circuiting, while the bare Li cell experienced severe overpotential increase after cycling for only  $\approx 300$  h, followed by failure at  $\approx 460$  h. Besides, the cycling overpotential value is  $\approx 25$  and  $\approx 100$  mV for LiAl-FBD coated Li and bare Li, respectively, demonstrating four-time lower polarization for the protected Li (Figure 2d). Even at higher current density, the overpotential of LiAl-FBD coated cell is maintained to be low (Figure S9, Supporting Information). These facts prove that LiAl-FBD can effectively prevent the Li metal corrosion caused by liquid electrolytes. Combined with the high ionic conductivity of the ASEI, stable impedance and cycling of Li metal anodes can be achieved. To further confirm the electrolyte-phobic nature of LiAl-FBD, the crystal was immersed in either carbonate (LP30) or ether electrolyte (4 M LiFSI/DME<sup>[38]</sup>) used in this work for 24 h, after which the <sup>1</sup>H- and <sup>19</sup>F-NMR were performed and they demonstrated negligible dissolution of LiAl-FBD species (Figure S10, Supporting Information).

The Li | Cu cells were further studied to show the impact of LiAl-FBD coating on cycling stability and Li metal CE. Different from the thick Li foils in Li | Li symmetric cells, the practical, industrial 50  $\mu$ m thin Li was used here to examine the

practicality of implementing LiAl-FBD coating in realistic battery structures. The voltage curve in Figure 2e showed severe fluctuation existed in the Li | bare Cu cell, especially during the initial and end stage of cycling which indicate the poor passivation capability of native SEI generated by a liquid electrolyte. On the contrary, the Li | LiAl-FBD@Cu cell showed more stable cycling plateau and longer cycle life than the bare Cu one, confirming the LiAl-FBD protection for Li metal cycling. As expected, the extracted CEs of two replicated Li | LiAl-FBD@Cu half cells (filled and hollow blue dots in Figure 2f) are consistently high ( $>97.5\%$ ). Although the Li | bare Cu cell showed slightly higher CE for the initial  $\approx 10$  cycles (Figure 2f), this probably results from the artifact induced by the voltage fluctuation at the initial cycling stage (Figure 2e). Considering these noises in voltage plateau, the Li | bare Cu half cell still falls short compared to the LiAl-FBD protected one. The Aurbach CE protocol<sup>[39,40]</sup> tests and Li | Cu half-cell cycling under other conditions confirmed our argument by showing superior performance for LiAl-FBD@Cu (Figure S11, Supporting Information).

To further understand the protection effect of LiAl-FBD coating, we performed X-ray photoelectron spectroscopy (XPS) and SEM to examine SEI structure and Li metal deposition morphology, respectively. To avoid the influence of residue salts or LiAl-FBD coating, the samples were quickly washed with anhydrous DME to expose fresh surface before XPS and SEM experiments.

For bare Li metal, high contents of electrolyte-derived species were observed (Figure 3a,b). For example, Li<sub>x</sub>PO<sub>y</sub>F<sub>z</sub> and LiF are the decomposition products of LiPF<sub>6</sub> salt while Li<sub>2</sub>CO<sub>3</sub> and Li<sub>2</sub>O are those derived from carbonate solvents. Moreover, the species vastly varied with depth profiling and such a vertically nonuniform feature along with the severe electrolyte degradation may be responsible for the poor performance of bare Li. By contrast, XPS spectra of LiAl-FBD@Li showed distinct behavior where FBD-based species dominated in both O1s and F1s spectra (Figure 3c,d). Electrolyte-decomposed products were not observed under LiAl-FBD protection, indicating its excellent electrolyte-blocking capability. It is worth noting that LiF was also found in LiAl-FBD coated Li (Figure 3d); however, it is uniformly distributed with different depths. The LiF species may primarily stem from well-controlled reaction<sup>[24]</sup> between FBD ligands and Li metal, and such a vertical uniformity was proved to be beneficial to Li metal cyclability.<sup>[22,41]</sup> The XPS of other elements and after long cycling supported our argument (Figures S12–S14, Supporting Information).

Li deposition morphology is another critical factor to correlate Li metal stability with ASEI protection effect. The Li deposits on bare Cu were dendritic as expected when using the carbonate electrolyte (Figure 3e and Figure S15a–c, Supporting Information); however, the deposition morphology was drastically improved with the LiAl-FBD ASEI, underneath which chunky Li deposits were dominant while needle-like Li filaments were completely absent (Figure 3f and Figure S15d,e, Supporting Information). The energy-dispersive X-ray spectra (EDS) showed uniformly distributed F and Al elements on Li metal deposit surface although DME solvent had washed most of the LiAl-FBD coating off (Figure 3g,h). This not only confirmed the planar uniform distribution of LiAl-FBD

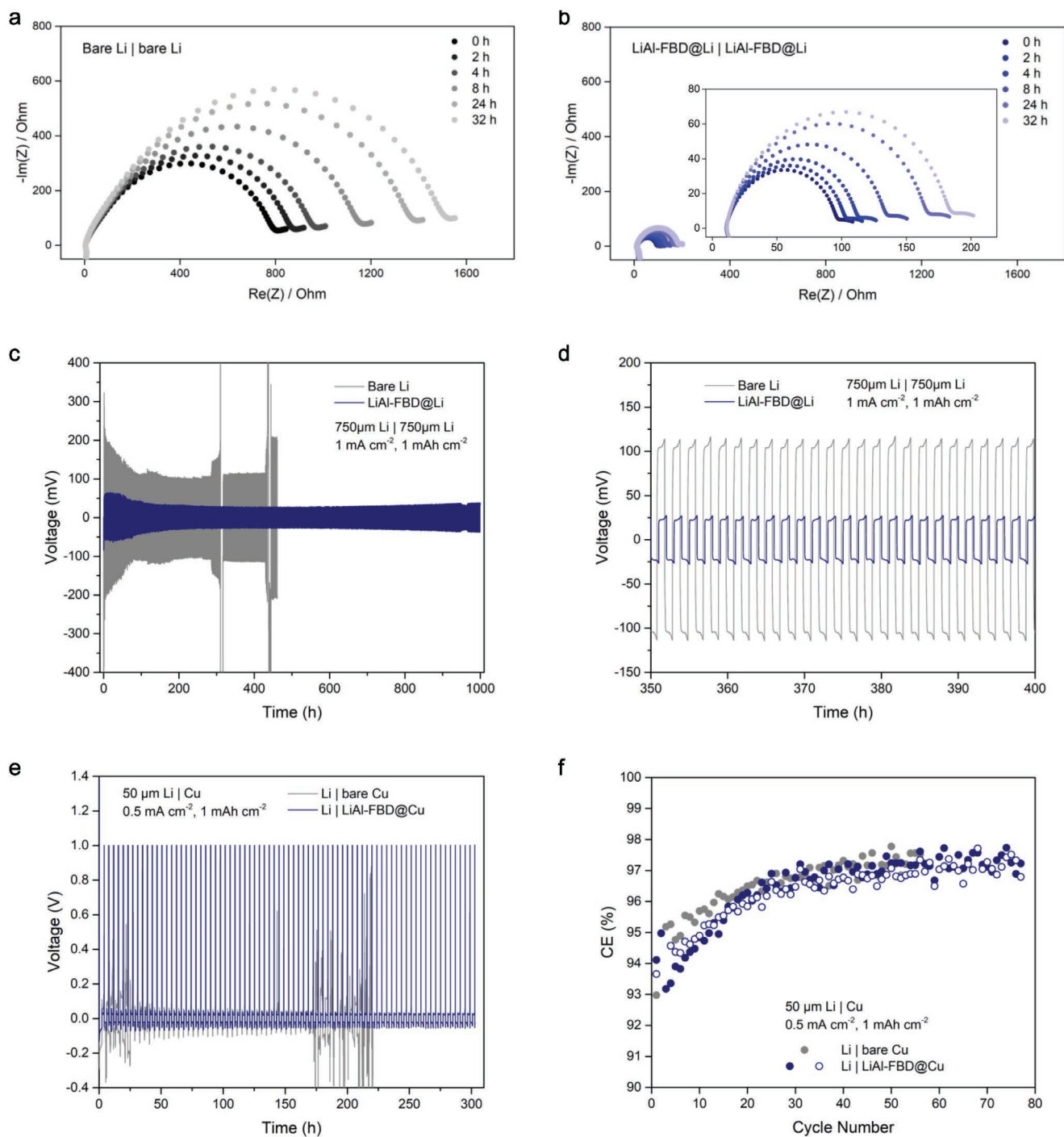


**Figure 2.** a,b) Impedance evolution of a) bare Li | bare Li and b) LiAl-FBD@Li | LiAl-FBD@Li symmetric cells over time. c,d) Cycling performance of bare Li | bare Li and LiAl-FBD@Li | LiAl-FBD@Li symmetric cells. d) A portion of (c) to enable visualization of the overpotential difference. e) Cycling curves of 50  $\mu\text{m}$  thick Li | bare Cu and 50  $\mu\text{m}$  thick Li | LiAl-FBD@Cu half cells in (e). Replicated results for LiAl-FBD@Cu are shown in (f). All the cells used 1 M LiPF<sub>6</sub> in EC/DMC (LP30) + 2% VC + 10% FEC as the electrolyte.

coating, but also corroborates with the XPS Al2p results (Figures S12e and S14e, Supporting Information) to show good contact between the ASEI and Li metal layer.

Although after long cycling the LiAl-FBD coating layer disintegrated and became less conformal, the coating was still found to adhere the surface of almost each Li deposit, serving as a

functional ASEI (Figure 3i–l and Figure S16, Supporting Information). Particularly, as shown in Figure 3l and Figure S16f (Supporting Information), the Li deposits (after 50 cycles) were densely packed underneath the LiAl-FBD layer (the top part between the light blue lines and the layer was curled up due to peeling off), confirming its protection effect even after

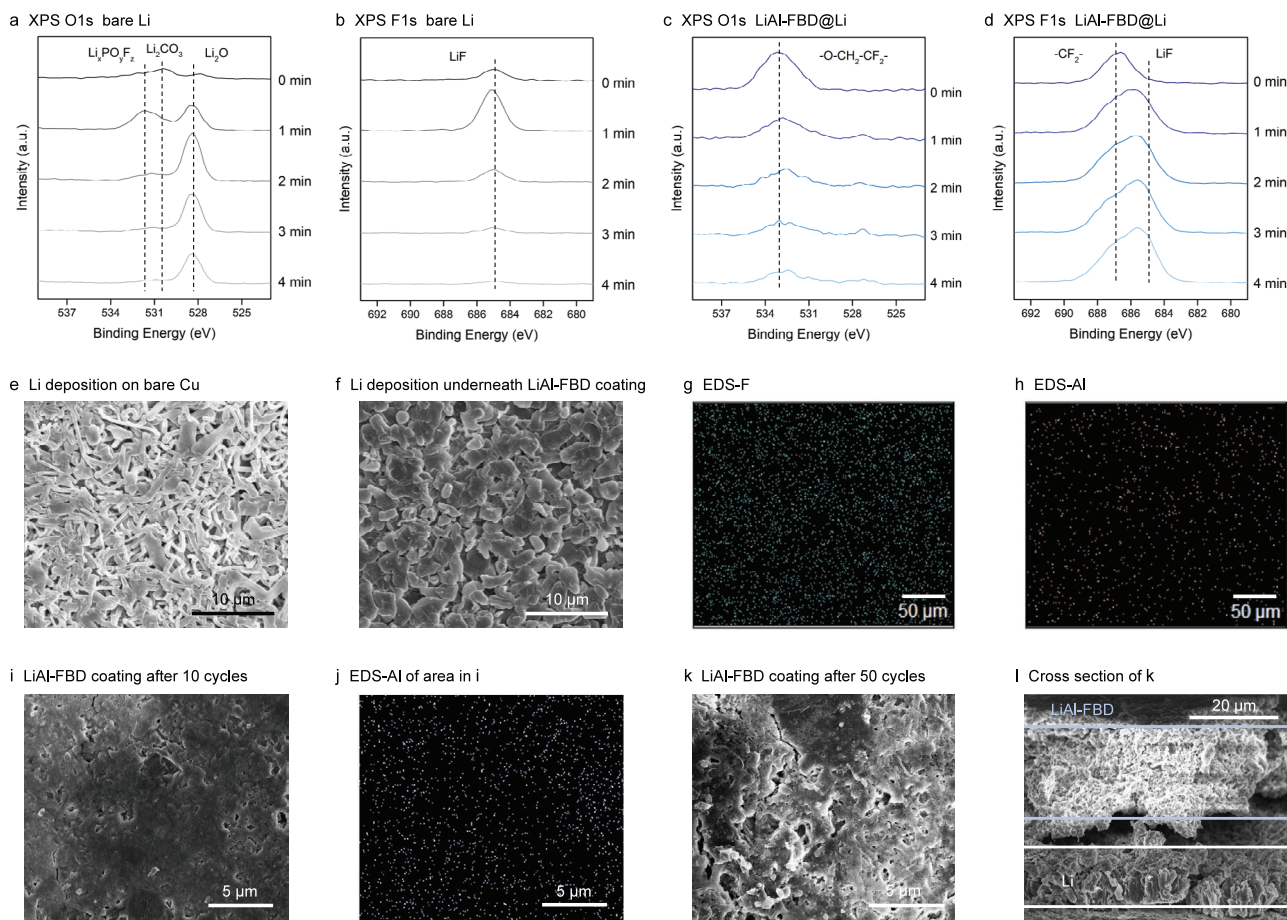


**Figure 3.** XPS of a,b) bare Li and c,d) LiAl-FBD coated Li soaked in the carbonate electrolyte for 4 days. e,f) Li deposits at  $0.5 \text{ mA cm}^{-2}$  current density and  $1 \text{ mAh cm}^{-2}$  areal capacity on e) bare Cu and f) underneath LiAl-FBD coating. EDS images showing g) F and h) Al element distribution on the Li surface underneath LiAl-FBD coating. SEM and EDS images of LiAl-FBD@Cu (with Li deposits underneath) after i,j) 10 or k,l) 50 cycles in the Li | Cu half cells.

long-term cycling. For further improvement of protection effects, dynamic materials such as viscoelastic polymers can be combined with LiAl-FBD to form composite, integrating dynamic and even healing properties.

Finally, we assembled practical Li metal full batteries to investigate the effectiveness of LiAl-FBD coating under more realistic conditions. Thin Li foil ( $50 \mu\text{m}$  thick), commercial lithium nickel manganese cobalt oxide cathode sheets with high loadings ( $2 \text{ mAh cm}^{-2}$  NMC532 from a commercial source and  $3.5 \text{ mAh cm}^{-2}$  NMC811 provided by Hyundai Motor Company), lean electrolyte amount ( $30$  or  $10 \mu\text{L cell}^{-1}$ , i.e., electrolyte-to-cathode ratio was  $15 \mu\text{L mAh}^{-1}$  for NMC532 and  $2.8 \mu\text{L mAh}^{-1}$  for NMC811), and high cycling current ( $0.6 \text{ mA cm}^{-2}$  for NMC532 cells and  $1 \text{ mA cm}^{-2}$  for NMC811 ones) were implemented here to fulfill practical testing conditions.

Commercial carbonate electrolyte, LP30 + 2% VC + 10% FEC, was first used. As shown in **Figure 4a**, the bare Li full cell suffered from sharp decay at  $\approx 100$  cycles, which has been identified as a phenomenon resulting from unstoppable Li/electrolyte parasitic reactions and thus electrolyte depletion.<sup>[42]</sup> **Figure 4b** shows that the LiAl-FBD@Li | NMC532 full cells possessed stable cycle life, and over 60% of original capacity was retained after 200 cycles. No drastic decrease in capacity

was observed, and therefore, the LiAl-FBD ASEI effectively protected the Li metal anode and prevented continuous corrosion or electrolyte depletion.<sup>[42]</sup> This difference in cycling behavior corroborates well with the observations in EIS evolution (**Figure 2a–d**) and XPS (**Figure 3a–d**). Consistent with the capacity retention trend, the CE of bare Li | NMC532 full cell started to fluctuate intensively from 100 cycles, while the CE was kept stable ( $\approx 100\%$ ) over the whole cycle life (**Figure 4b**). To further push the cycling performance, high-concentration ether-based electrolyte,  $4 \text{ M LiFSI/DME}$ ,<sup>[38]</sup> was implemented. The bare Li | NMC811 cell experienced sudden capacity dive after  $\approx 130$  cycles, and it was when the full-cell CE started to significantly fluctuate (**Figure 4c,d**). By contrast, the LiAl-FBD@Li | NMC811 cell was stably cycled for  $\approx 200$  cycles followed by gradual capacity fading until  $\approx 250$  cycles (**Figure 4c**). Such a slow decay is consistent with the LiAl-FBD@Li | NMC532 cell results and again confirms the protection effect of LiAl-FBD ASEI. The CE of the LiAl-FBD cell was maintained at  $\approx 100\%$  for  $>230$  cycles before fluctuation (**Figure 4d**). When other electrolyte recipes and cycling conditions were applied, the LiAl-FBD@Li cells all showed better performance than bare ones and our previously reported dynamic, single-ion-conductive and electrolyte-blocking coating,<sup>[24]</sup> and these performances also

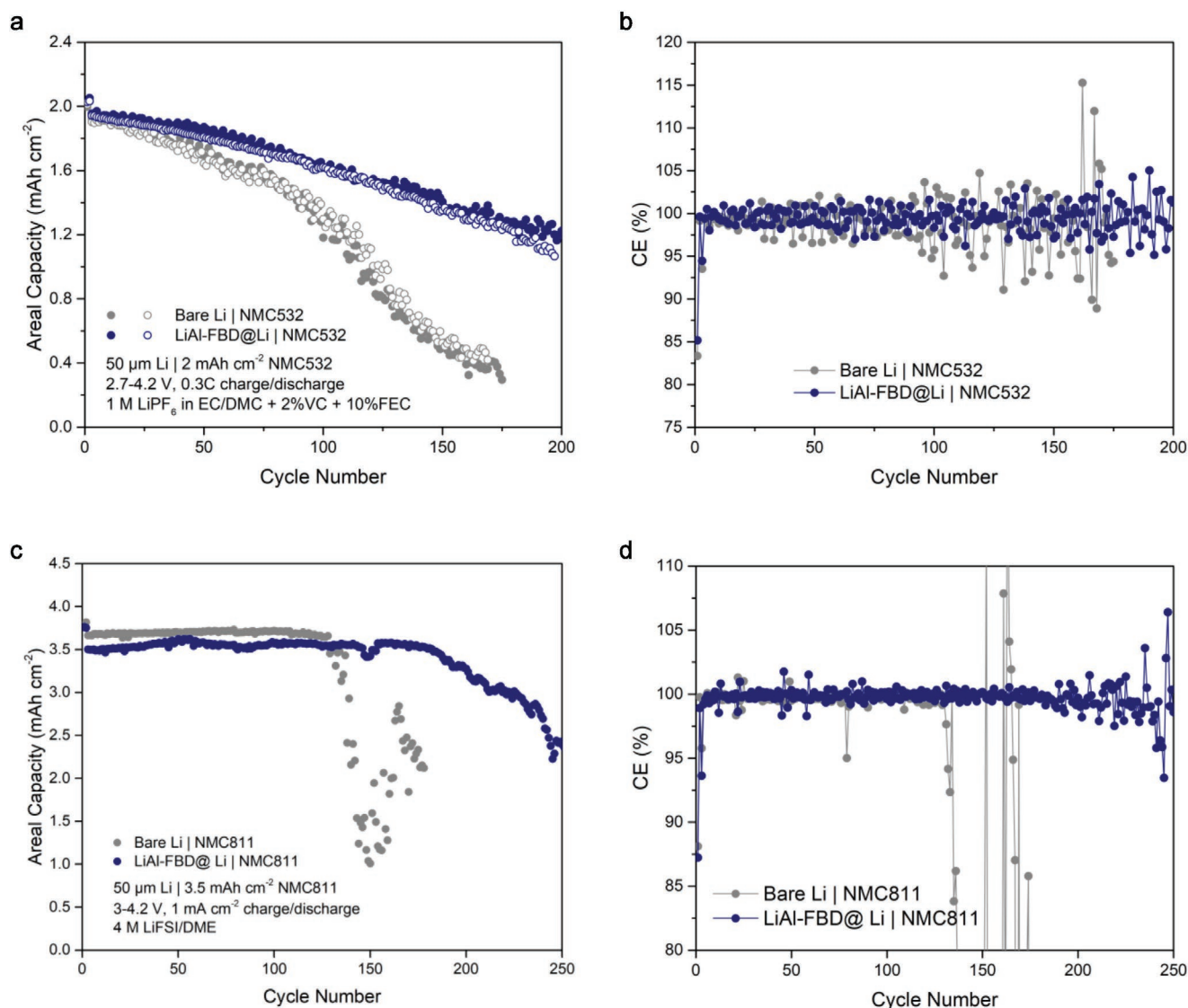


**Figure 4.** a,b) Full cell performance and corresponding CE evolution using 50 μm thick Li, commercial NMC532 cathode sheet, and commercial carbonate electrolyte. Replicated results for bare Li and LiAl-FBD@Li cells are shown here. c,d) Full cell performance and corresponding CE evolution using 50 μm thick Li, industrial NMC811 cathode sheet (provided by Hyundai Motor Company), and high-concentration ether electrolyte. Replicated cells are shown here and in Figures S14 and S15 (Supporting Information).

stand high among other artificial coating strategies (Figures S17 and S18 and Table S1, Supporting Information).

### 3. Conclusions

In summary, we designed and synthesized a mechanically robust ASEI, LiAl-FBD, that can be solution processed readily on Li foil. Its single-crystal structure was solved and demonstrated to be Li<sub>3</sub>Al<sub>3</sub>(FBD)<sub>6</sub>(DME)<sub>3</sub>, in which Al<sup>3+</sup> ions were bridged by FBD<sup>2-</sup> ligands to form the anion-cluster while Li<sup>+</sup> ions were loosely bound and located at the periphery. Such a structure, along with high Li<sup>+</sup> content due to short ligands, enabled good ion transport. In addition, the highly fluorinated ligands endowed the ASEI with electrolyte phobicity. Careful

characterizations such as nanoindentation, XPS, SEM, EIS, Li | Li symmetric cell cycling and Li metal CE showed that LiAl-FBD is a mechanically strong, electrolyte blocking, and ion-conductive coating to well protect the Li metal anode. The Li metal batteries using LiAl-FBD coated thin Li foil, commercial or industrial NMC high-loading high-voltage cathodes, and lean electrolyte conditions showed superior cycling performance than bare Li cells, confirming the practicality of using this solution-processable ASEI in realistic Li metal batteries.

### Supporting Information

Supporting Information is available from the Wiley Online Library or from the author.

## Acknowledgements

This work is supported by Hyundai Motor Company (HMC). Part of this work was performed at the Stanford Nano Shared Facilities (SNSF), supported by the National Science Foundation under award ECCS-2026822. Use of the Stanford Synchrotron Radiation Lightsource (SSRL), SLAC National Accelerator Laboratory, is supported by the U.S. Department of Energy, Office of Science, Office of Basic Energy Sciences under Contract No. DE-AC02-76SF00515.

## Conflict of Interest

A joint patent between Stanford University and Hyundai Motor Company is filed.

## Authors Contribution

Z.Y., S.S., J.S., and Z.B. conceived the idea. S.S., W.K., K.R., and Z.B. initiated and directed the project. Z.Y., S.S., and J.S. designed the logical flow and experiments. Z.Y. performed syntheses, material characterizations, electrochemical measurements, and battery tests. Z.Z., H.G., and Y.T. took SEM and EDS images. S.T.O. collected XPS data. Y.W. and R.X. helped with nanoindentation measurement. S.Z. and Y.Z. performed GIWAXS and analyses. L.M. and, E.G.L. helped with syntheses and part of electrochemical tests. X.W. refined crystal structure. S.S. and J.S. contributed to key discussions. W.K. and K.R. managed funding. Z.Y., S.S., and Z.B. cowrote and revised the manuscript. All authors discussed and approved the manuscript.

## Data Availability Statement

The data that support the findings of this study are available from the corresponding author upon reasonable request.

## Keywords

ASEI, crystalline, high modulus, Li metal batteries, solution processable

Received: March 24, 2022

Revised: May 16, 2022

Published online: June 28, 2022

- [1] J. Liu, Z. Bao, Y. Cui, E. J. Dufek, J. B. Goodenough, P. Khalifah, Q. Li, B. Y. Liaw, P. Liu, A. Manthiram, Y. S. Meng, V. R. Subramanian, M. F. Toney, V. V. Viswanathan, M. S. Whittingham, J. Xiao, W. Xu, J. Yang, X. Yang, J. Zhang, *Nat. Energy* **2019**, *4*, 180.
- [2] Y. Cao, M. Li, J. Lu, J. Liu, K. Amine, *Nat. Nanotechnol.* **2019**, *14*, 200.
- [3] X.-B. Cheng, R. Zhang, C.-Z. Zhao, F. Wei, J.-G. Zhang, Q. Zhang, *Adv. Sci.* **2016**, *3*, 1500213.
- [4] M. D. Tikekar, S. Choudhury, Z. Tu, L. A. Archer, *Nat. Energy* **2016**, *1*, 16114.
- [5] D. Lin, Y. Liu, Y. Cui, *Nat. Nanotechnol.* **2017**, *12*, 194.
- [6] X. He, D. Bresser, S. Passerini, F. Baakes, U. Krewer, J. Lopez, C. T. Mallia, Y. Shao-Horn, I. Cekic-Laskovic, S. Wiemers-Meyer, F. A. Soto, V. Ponce, J. M. Seminario, P. B. Balbuena, H. Jia, W. Xu, Y. Xu, C. Wang, B. Horstmann, R. Amine, C.-C. Su, J. Shi, K. Amine, M. Winter, A. Latz, R. Kostecki, *Nat. Rev. Mater.* **2021**, *6*, 1036.
- [7] G. M. Hobold, J. Lopez, R. Guo, N. Minafra, A. Banerjee, Y. S. Meng, Y. Shao-horn, B. M. Gallant, *Nat. Energy* **2021**, *6*, 951.
- [8] B. Flamme, G. R. Garcia, M. Weil, M. Haddad, P. Phansavath, V. Ratovelomanana-Vidal, A. Chagnes, *Green Chem.* **2017**, *19*, 1828.
- [9] H. Wang, Z. Yu, X. Kong, S. C. Kim, D. T. Boyle, J. Qin, Z. Bao, Y. Cui, *Joule* **2022**, *6*, 588.
- [10] N. Aspern, G.-V. Rösenthaller, M. Winter, I. Cekic-Laskovic, *Angew. Chem., Int. Ed.* **2019**, *58*, 15978.
- [11] X. Fan, C. Wang, *Chem. Soc. Rev.* **2021**, *50*, 10486.
- [12] M. S. Kim, Z. Zhang, P. E. Rudnicki, Z. Yu, J. Wang, H. Wang, S. T. Oyakhire, Y. Chen, S. C. Kim, W. Zhang, D. T. Boyle, X. Kong, R. Xu, Z. Huang, W. Huang, S. F. Bent, L. Wang, J. Qin, Z. Bao, Y. Cui, *Nat. Mater.* **2022**, *21*, 445.
- [13] Y. Chen, Z. Yu, P. Rudnicki, H. Gong, Z. Huang, S. C. Kim, J. Lai, X. Kong, J. Qin, Y. Cui, Z. Bao, *J. Am. Chem. Soc.* **2021**, *143*, 18703.
- [14] L. Tan, S. Chen, Y. Chen, J. Fan, D. Ruan, Q. Nian, L. Chen, S. Jiao, X. Ren, *Angew. Chem., Int. Ed.* **2022**, <https://doi.org/10.1002/anie.202203693>.
- [15] J. Li, Y. Cai, H. Wu, Z. Yu, X. Yan, Q. Zhang, T. Z. Gao, K. Liu, X. Jia, Z. Bao, *Adv. Energy Mater.* **2021**, *11*, 2003239.
- [16] J. W. Fergus, *J. Power Sources* **2010**, *195*, 4554.
- [17] Y. Lin, Y. Chen, Z. Yu, Z. Huang, J. C. Lai, J. B. H. Tok, Y. Cui, Z. Bao, *Chem. Mater.* **2022**, *34*, 2393.
- [18] Y. Ma, J. Wan, Y. Yang, Y. Ye, X. Xiao, D. T. Boyle, W. Burke, Z. Huang, H. Chen, Y. Cui, Z. Yu, S. T. Oyakhire, Y. Cui, *Adv. Energy Mater.* **2022**, *12*, 2103720.
- [19] H. Wang, Y. Liu, Y. Li, Y. Cui, *Electrochem. Energy Rev.* **2019**, *2*, 509.
- [20] N. Li, Y. Yin, C. Yang, Y. Guo, *Adv. Mater.* **2016**, *28*, 1853.
- [21] Y. J. Zhang, W. Wang, H. Tang, W. Q. Bai, X. Ge, X. L. Wang, C. D. Gu, J. P. Tu, *J. Power Sources* **2015**, *277*, 304.
- [22] H. Chen, A. Pei, D. Lin, J. Xie, A. Yang, J. Xu, K. Lin, J. Wang, H. Wang, F. Shi, D. Boyle, Y. Cui, *Adv. Energy Mater.* **2019**, *9*, 1900858.
- [23] M. S. Kim, J.-H. Ryu, Deepika, Y. R. Lim, I. W. Nah, K.-R. Lee, L. A. Archer, W. Il Cho, *Nat. Energy* **2018**, *3*, 889.
- [24] Z. Yu, D. G. Mackanic, W. Michaels, M. Lee, A. Pei, D. Feng, Q. Zhang, Y. Tsao, C. V. Amanchukwu, X. Yan, H. Wang, S. Chen, K. Liu, J. Kang, J. Qin, Y. Cui, Z. Bao, *Joule* **2019**, *3*, 2761.
- [25] Z. Huang, S. Choudhury, H. Gong, Y. Cui, Z. Bao, *J. Am. Chem. Soc.* **2020**, *142*, 21393.
- [26] X. Chen, M. Shang, J. Niu, *ACS Appl. Mater. Interfaces* **2021**, *13*, 34064.
- [27] Y. Gao, Z. Yan, J. L. Gray, X. He, D. Wang, T. Chen, Q. Huang, Y. C. Li, H. Wang, S. H. Kim, T. E. Mallouk, D. Wang, *Nat. Mater.* **2019**, *18*, 384.
- [28] Z. Huang, S. Choudhury, N. Paul, J. H. Thienenkamp, P. Lennartz, H. Gong, P. Müller-Buschbaum, G. Brunklau, R. Gilles, Z. Bao, *Adv. Energy Mater.* **2022**, *12*, 2103187.
- [29] H. Liu, X. Cheng, Y. Chong, H. Yuan, J.-Q. Huang, Q. Zhang, *Particulateology* **2021**, *57*, 56.
- [30] Z. Bao, Z. Yu, D. Feng, M. A. Lee, Y. Cui, A. Pei, *US 2022/0017431 A1*, **2022**.
- [31] R. Xu, X. Cheng, C. Yan, X.-Q. Zhang, Y. Xiao, C. Zhao, J.-Q. Huang, Q. Zhang, *Matter* **2019**, *1*, 317.
- [32] Z. Yu, Y. Cui, Z. Bao, *Cell Rep. Phys. Sci.* **2020**, *1*, 100119.
- [33] H. Zhou, S. Yu, H. Liu, P. Liu, *J. Power Sources* **2020**, *450*, 227632.
- [34] J. Lopez, A. Pei, J. Y. Oh, G.-J. N. Wang, Y. Cui, Z. Bao, *J. Am. Chem. Soc.* **2018**, *140*, 11735.
- [35] L. Li, G. Xu, S. Zhang, S. Dong, S. Wang, Z. Cui, X. Du, C. Wang, B. Xie, J. Du, X. Zhou, G. Cui, *ACS Energy Lett.* **2022**, *7*, 591.
- [36] Y. Liu, Y.-K. Tzeng, D. Lin, A. Pei, H. Lu, N. A. Melosh, Z.-X. Shen, S. Chu, Y. Cui, *Joule* **2018**, *2*, 1595.
- [37] Y. Zhao, G. Li, Y. Gao, D. Wang, Q. Huang, D. Wang, *ACS Energy Lett.* **2019**, *4*, 1271.
- [38] J. Qian, W. A. Henderson, W. Xu, P. Bhattacharya, M. Engelhard, O. Borodin, J.-G. Zhang, *Nat. Commun.* **2015**, *6*, 6362.

- [39] D. Aurbach, Y. Gofer, J. Langzam, *J. Electrochem. Soc.* **1989**, *136*, 3198.
- [40] B. D. Adams, J. Zheng, X. Ren, W. Xu, J.-G. Zhang, *Adv. Energy Mater.* **2018**, *8*, 1702097.
- [41] Z. Yu, P. E. Rudnicki, Z. Zhang, Z. Huang, H. Celik, S. T. Oyakhire, Y. Chen, X. Kong, S. C. Kim, X. Xiao, H. Wang, Y. Zheng, G. A. Kamat, M. S. Kim, S. F. Bent, J. Qin, Y. Cui, Z. Bao, *Nat. Energy* **2022**, *7*, 94.
- [42] C. Niu, D. Liu, J. A. Lochala, C. S. Anderson, X. Cao, M. E. Gross, W. Xu, J. Zhang, M. S. Whittingham, J. Xiao, J. Liu, *Nat. Energy* **2021**, *6*, 723.